

Atlantic inflow is the primary driver of remotely sensed autumn blooms in the Barents Sea.

Andrew Orkney^{*1}, Shubha Sathyendranath^{2,3}, Thomas Jackson²,
Marie Porter⁴ & Heather A. Bouman¹

Andrew Orkney: <https://orcid.org/0000-0003-4972-2541>

Shubha Sathyendranath: <https://orcid.org/0000-0003-3586-192X>

Thomas Jackson: <https://orcid.org/0000-0003-4336-1597>

Marie Porter: <https://orcid.org/0000-0003-3686-353X>

Heather A. Bouman: <https://orcid.org/0000-0002-7407-9431>

1: Department of Earth Sciences, University of Oxford, OX1 3AN

2: Plymouth Marine Laboratory, PL1 3DH

3: National Centre for Earth Observation, Plymouth Marine Laboratory, PL1 3DH

4: Scottish Association for Marine Science,
Scottish Marine Institute, Oban, PA37 1QA

Running page head: Barents Sea autumn bloom dynamics

Key words: Arctic; Atlantification; Climate change; Ocean colour;
Phenology; Phytoplankton

October 26, 2022

Contents

1	Text S1	2
1.1	Confounding factors affecting remotely sensed chlorophyll concentration	2
1.2	Parallel analysis without masking coccolithophores	3
1.3	Additional analyses	3
2	Tables	5
3	Figures	6
4	LITERATURE CITED	12

* Corresponding author: saxon.wessex.orkney@gmail.com

1 Text S1

1.1 Confounding factors affecting remotely sensed chlorophyll concentration

We rotated ocean-colour data onto a set of two new axes by multiplying the 6 *Rrs* OC-CCIv5 remotely sensed reflectance values by wavelength specific (λ) coefficients (a_i), summing, and subtracting a constant (b_i);

$$S_i = (\sum_{\lambda=1}^6 a_{i\lambda} Rrs_{\lambda}) - b_i, \quad (\text{Equation S1})$$

where S_i is the result, a_i represents the slew of coefficients and b_i is a constant.

Two sets of values were used (Table S1), such that two series of values, S_1 and S_2 were defined. Thereafter all ocean-colour data, for which $S_2 > -0.5 S_1 + 0.0015$ and $S_2 < 0.4 S_1 + 0.003$, were considered to represent coccolithophores and masked. An example of the application of this algorithm to ocean-colour data is provided in Figure S1.

Prior to analysis we examined the relationship between retrieved $[chl-a]$ and sample completeness, to explore potential sources of bias in remotely sensed $[chl-a]$ integrations. We derived a sampling completeness ‘coverage metric’, by recording the number of unique latitude-longitude combinations perceived in any September. Should a persistent ice or cloud field be present that may obscure a bloom, we should expect a relationship between average monthly $[chl-a]$ inferred by remote sensing and variation in the coverage metric. A significant increase in average monthly $[chl-a]$ values is evident across our time series (main manuscript Figure 4d), consistent with reports of increasing biomass in the Barents Sea (e.g. Lewis et al. (2020), Siswanto (2020)), but is this driven by variation in coverage? Overall, simple linear regressions between $[chl-a]$ and coverage metric, and their inter-annual differences, are not associated with high R^2 values or low p-values (secular trends: $R^2 = 0.1641$, $p = 0.0537$, interannual differences: $R^2 = 0.067$, $p = 0.164$). This shows that satellite data coverage is unlikely to distort patterns of secular change in September $[chl-a]$.

The results of time-series analysis show that there are not only relationships between secular trends among the different variables, but that there are also lagged relationships (main manuscript Figure S4d), illustrating complex multi-annual resonances and feedbacks. For example, in a simple linear regression, variation in the storminess index is significantly related to the coverage metric of the previous year ($p = 0.014$). This could be consistent with a hypothetical positive ‘wind loop’ feedback, whereby high Atlantic inflow causes high open ocean area, hence a high coverage metric, and thereby facilitates greater loss of oceanic heat to the atmosphere. This results in low-pressure systems that draw in further strong westerly winds (Smedsrud et al. 2013). It can also be seen that storminess and SST excursions anti-correlate, consistent with higher winds engendering greater open ocean area and vertical mixing, enhancing heat loss to the atmosphere.

Thus, while coverage does not directly distort inferred $[chl-a]$, it may influence multi-annual relationships and feedbacks between $[chl-a]$ and environmental drivers. The potential bias that coverage has in the perception of mean monthly $[chl-a]$ cannot therefore be easily disentangled from potential mechanistic drivers of $[chl-a]$ variance without the use of repeated in-situ measurements. We conclude that it is best not to endeavour to remove signal associated with variation in coverage for this reason. However, we do note that, given multi-annual feedbacks between environmental variables are evident, that it is necessary to account for temporal autocorrelation before the mechanistic drivers of autumn $[chl-a]$ variation can be deciphered.

1.2 Parallel analysis without masking coccolithophores

A parallel analysis was undertaken, in which no effort was made to remove the effects of calcifying coccolithophore blooms on the inference of $[chl-a]$ from ocean colour. Secular trends in inferred $[chl-a]$ and dependencies of $[chl-a]$ upon environmental variables are presented in Figures S2–S4. GLS models were also computed, and those which differ from the main manuscript (Table 2) are presented in Table S2.

The inclusion of coccolithophore blooms results in a slight reduction of the number of grid-cells assessed to have significant secular increases in $[chl-a]$. This change is especially apparent in the central Barents Sea (Figure S2a). We note that coccolithophore blooms have slowly been occurring further east, as a result of the ongoing Atlantification of the Barents Sea (e.g. Oziel et al. (2017), Oziel et al. (2020), Orkney et al. (2020)). While coccolithophore blooms rarely occurred east of 40° in the 20th Century, they may now occur as far east as the coast of Novaya Zemlya (see Figure S1). A change in the spatial distribution of coccolithophore blooms could perhaps explain why a secular increase in $[chl-a]$ is not identified in the central Barents Sea in Figure S2a.

The south-east Barents Sea, where coccolithophore blooms have become increasingly common, exhibits a clearer dependency of $[chl-a]$ upon SST (compare Figures S3a and 3a). This is consistent with reports of an increasing occurrence of coccolithophore blooms associated with the dispersal of warm Atlantic Water into the south-east Barents Sea (Neukermans et al. 2018, Oziel et al. 2020). In support of this interpretation, we observe that a greater number of grid-cells in the south-east Barents Sea support a dependency of $[chl-a]$ upon local current speed when coccolithophore blooms are not masked (compare Figures S3c and 3c). Overall, the decision to mask coccolithophores appears to have no substantial influence on perceived dependency of $[chl-a]$ upon windiness (compare Figures S3b and 3b), with the exception of a possible decline in the coefficient that relates these variables in the south-east Barents Sea. However, this region is not typified by low p-values that would indicate significance.

Dependencies of $[chl-a]$ upon average current speed in the south-western Barents Sea (C_i), appear to change little as a result of the inclusion of coccolithophores (compare Figures S4a and 4a). Nor does the relationship between their inter-annual differences change substantially (compare Figures S4b and 4b). The relationship between inter-annual differences in $[chl-a]$ and windiness is also changed little by the inclusion of coccolithophores (compare Figures S4c and 4c). An overall time-series of $[chl-a]$, normalised by its variance, does not appear to change considerably (compare Figures S4d and 4d). However, the difference between fit statistics describing GLS models relating $[chl-a]$ to SST and C_i , is more apparent in a comparison of Tables S2 and 2. This shows that the inclusion of coccolithophores results in a smaller difference in AICc values and p-values. We interpret this as a result of the stronger signal relating $[chl-a]$ and SST in the south-east Barents Sea, which manifests when coccolithophore blooms are included in assessments of $[chl-a]$.

In conclusion, our parallel analysis demonstrates that failure to distinguish calcifying coccolithophore blooms from non-calcifying Autumn blooms could subtly alter researcher perceptions about the environmental drivers of phytoplankton phenology in the Barents Sea.

1.3 Additional analyses

Additional visualisations of a selection of the model fits, presented in main manuscript Table 2, are illustrated in Figure S5. Points are coloured by year, to foster comprehension of the relationship between pairwise combinations of variables and their evolution with time. The plots

demonstrate significant positive dependencies of remotely sensed autumn $[chl-a]$ upon SST, average current speed in the south-western Barents Sea, and the frequency of windy days. The dependency upon current speed is clearest, and the distribution shows that this relationship is structured over time, with the most intense current speeds and highest inferred $[chl-a]$ occurring in more recent years (Figure S5b). We note that, at a synoptic scale, SST does not appear strongly related to windiness (Figure S5e). This masks subtler complexity at a regional scale (Figure S3d). A negative dependency of SST upon windiness is weakened when it is mixed with a positive relationship that exists north of the Polar Front, in Arctic dominated waters. This highlights the importance of inspecting geographically resolved relationships, as well as synoptic scale averages.

It is possible that bathymetry may impose geographic structure on secular trends in $[chl-a]$, or its response to environmental variables, within any grid-cell (Kogeler & Rey 1999). Testing this is not straightforward, because bathymetry is not randomly organised; it has its own variance structure that causes statistical non-independence. Hence, Ordinary Least Squares (OLS) fits (which do not accommodate sample non-independence) were compared against Generalised Least Squares fits, in which the residual covariance matrix represented sample non-independence structured over geography (spatial autocorrelation).

Variograms of the OLS fit residuals as a function of geography were computed with the `variogram` and `fit.variogram` functions of the R `gstat` package (Pebesma 2004). A radius of 11° was assumed as the scale over which range and nugget values were to be fitted. Thereafter, estimates for the range and nugget values were employed to produce a residual covariance matrix representing spatial autocorrelation with the `corSpher` argument in `gls` (Pinheiro et al. 2020). If estimated nugget ranges were unrealistic (< 0 or > 1) an estimate of 0.1 was substituted.

Neither OLS or GLS fits found a significant dependency of the slope of secular change in $[chl-a]$ upon the logarithm of the magnitude of bathymetry ($p = 0.15$ and $p = 0.13$, respectively) (Figure S6a). This implies that bathymetric features have not played a significant first-order role in determining secular change in autumn $[chl-a]$ across the Barents Sea.

For the dependency of $[chl-a]$ upon average current speed in the south-western Barents Sea, both OLS and GLS retrieve significant results ($p = 0.04$ and $p = 0.0003$, respectively) (Figure S6c). However the coefficient of the slopes of these models are antithetical (2.04 and -4.35). This may be because Atlantic Water in the south-west Barents Sea flows over areas of deeper basins and openings before entering the shelf. When spatial autocorrelation is not considered, deeper regions appear to exhibit a stronger relationship. When this geographic organisation is accounted for, deeper bathymetry appears less likely to support a stronger dependency of $[chl-a]$ upon inflow current speed.

Figure S6c provides further insight. There is a divergent distribution of points and no clear linear relationship. To explore further, we restricted our analysis to only those grid-cells which showed significant secular changes in $[chl-a]$ or significant dependencies of $[chl-a]$ upon inflow current speed, respectively. Both OLS and GLS fits found a significant negative dependency for the slope of secular change in $[chl-a]$ as a function of bathymetry ($p = 0.02$, $p = 0$, respectively) (Figure S6b). This indicates that, within the grid-cells which show a significant change in autumn $[chl-a]$ across the time series, shallower areas tend to show greater increases in $[chl-a]$. For the dependency of $[chl-a]$ upon average current speed in the south-western Barents Sea, OLS finds no significant dependency, but GLS retrieves significant results ($p = 0.53$ and $p = 0$, respectively) (Figure S6d). The slope of the GLS model is negative, indicating that shallower bathymetries tend to support a stronger dependency. In sum, the results of OLS and GLS model fits are variable and depend on how data is subsetting. This indicates that, if shallow bathymetry does have an effect enhancing secular trends in $[chl-a]$ or modulating

environmental dependencies, that this effect is subtle and does not substantially over-print other environmental dependencies.

2 Tables

Table S1: Wavelengths and coefficients employed to mask coccolithophores in ocean-colour data. $b_1 = 0.008820334$ and $b_2 = -0.0005476582$.

λ (nm)	412	443	490	510	560	665
a_1	0.47091009	0.48800140	0.49696639	0.43672448	0.31694570	0.04404408
a_2	-0.5822403	-0.3063442	0.1096942	0.3814065	0.6141931	0.1800353

Table S2: Summary of Generalised Least Squares model results, without masking coccolithophores. Rows: independent variables. Columns: dependent variables. Rows identical to Table 2 in the main manuscript are omitted.

B	SST	C_i	W
B	AICc = 49.15 p = 0.0013*	AICc = 45.10 p = 0.0002*	AICc _A ⁿ = 56.03 p = 0.027*

Note. GLS regressions fitted with the gls function, relating $[chl-a]$ (B), SST, inflow current speed (C_i) and the windy events index (W). An ‘A’ subscript indicates a lag-1 autocorrelated model is preferred at an alpha level of 0.05. ‘n’ superscripts indicate negative relationships, while ‘*’ denotes significance at a 0.05 alpha level. Model fits are described by their corrected Akaike Information Criterion (AICc) and p-values.

152 3 Figures

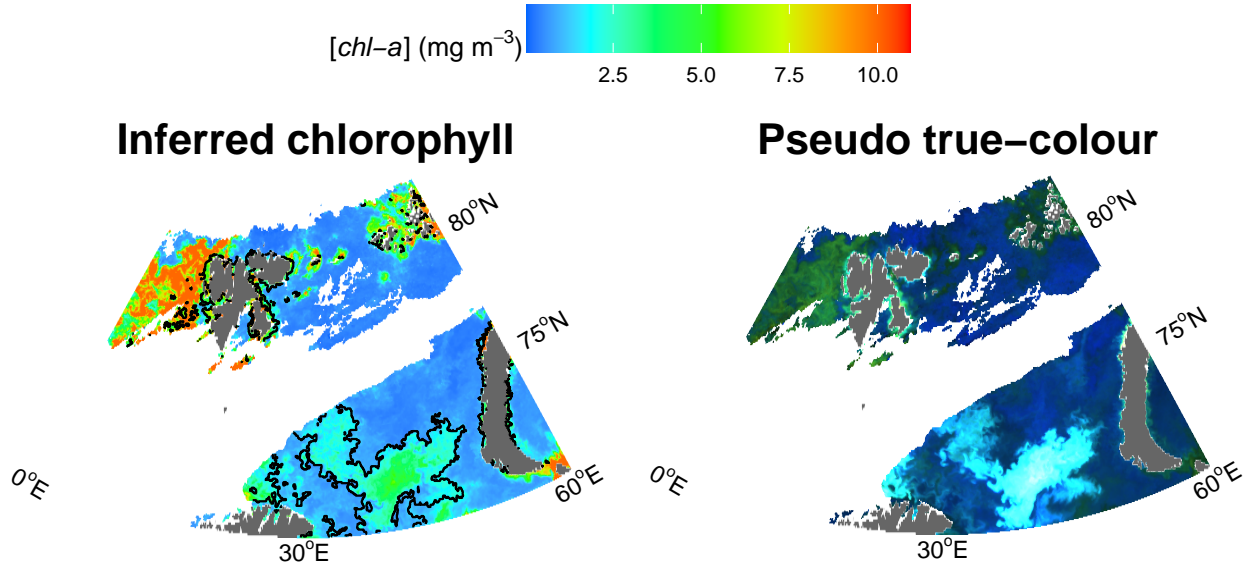


Figure S1: Maps of $[chl-a]$ inferred from application of OC6_meris to OC-CCIv5 data in the Barents Sea on the 6th of July 2016 (left) and a pseudo true-colour representation (right). An intense coccolithophore bloom is seen in the south-eastern Barents Sea (Hansen et al. 2016), and corresponds to a local high in inferred $[chl-a]$. Our custom coccolithophore mask is seen as a black contour in the left panel, correctly identifying this feature. $[chl-a]$ has been capped below 10 mg m^{-3} to aid visualisation.

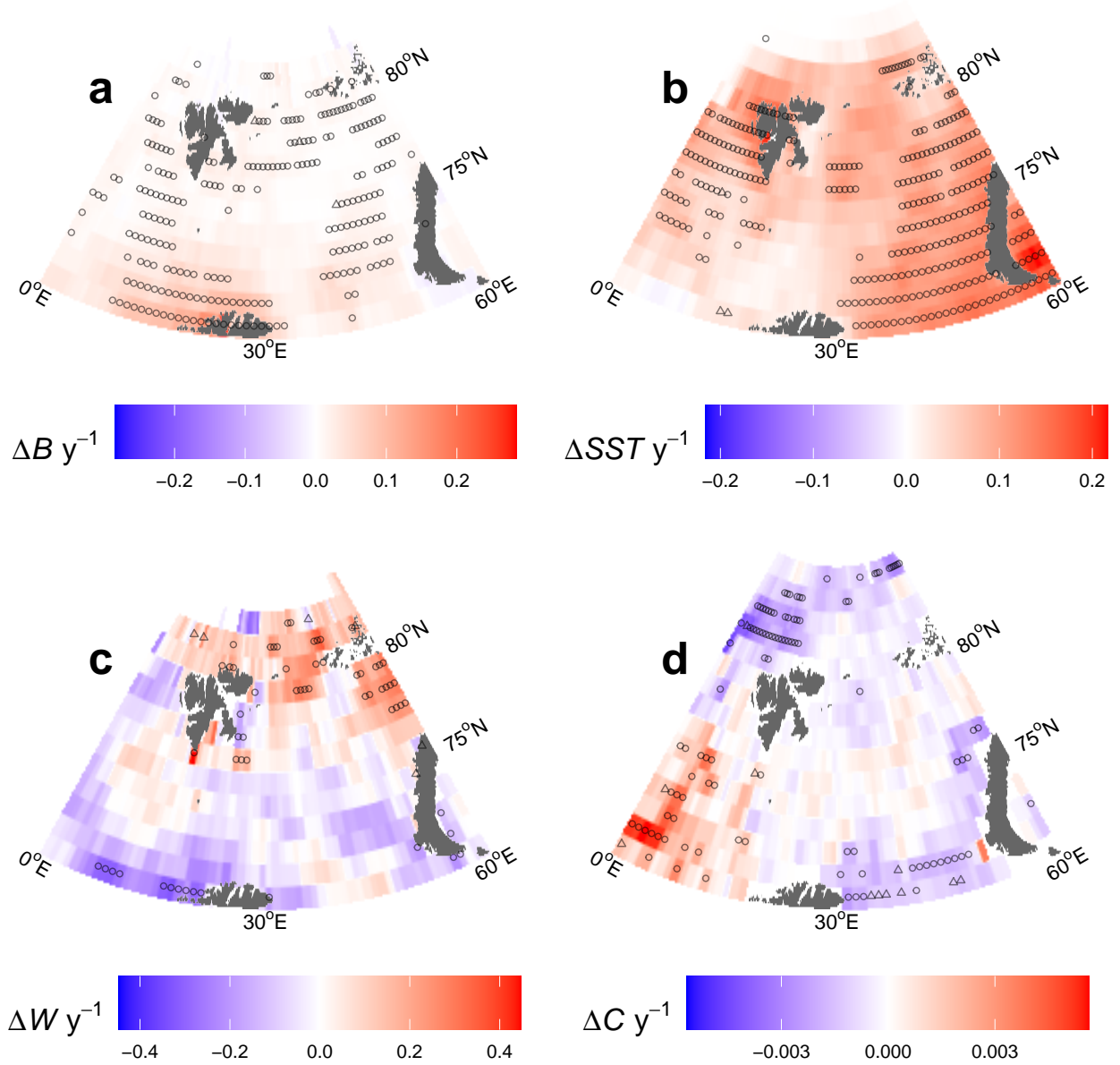


Figure S2: **Linear trends, without masking coccolithophores:** Slopes of linear models of the temporal evolution of [*chl-a*] (B) (mg m^{-3}), Sea Surface Temperature (SST) (Kelvin), windy days (W) and current speed (C) (ms^{-1}), for September between 2002 and 2019. **a)** Biomass **b)** SST **c)** Windy days **d)** Current speeds. Grid cells with significant ($p < 0.05$) trends are marked with triangles when an autocorrelated fit is preferred, and circles when a standard fit is preferred. Secular increases in biomass and SST are evident. Trends in windy days and current speeds show regional complexity. All data represent monthly integrations in September between 2002 and 2019.

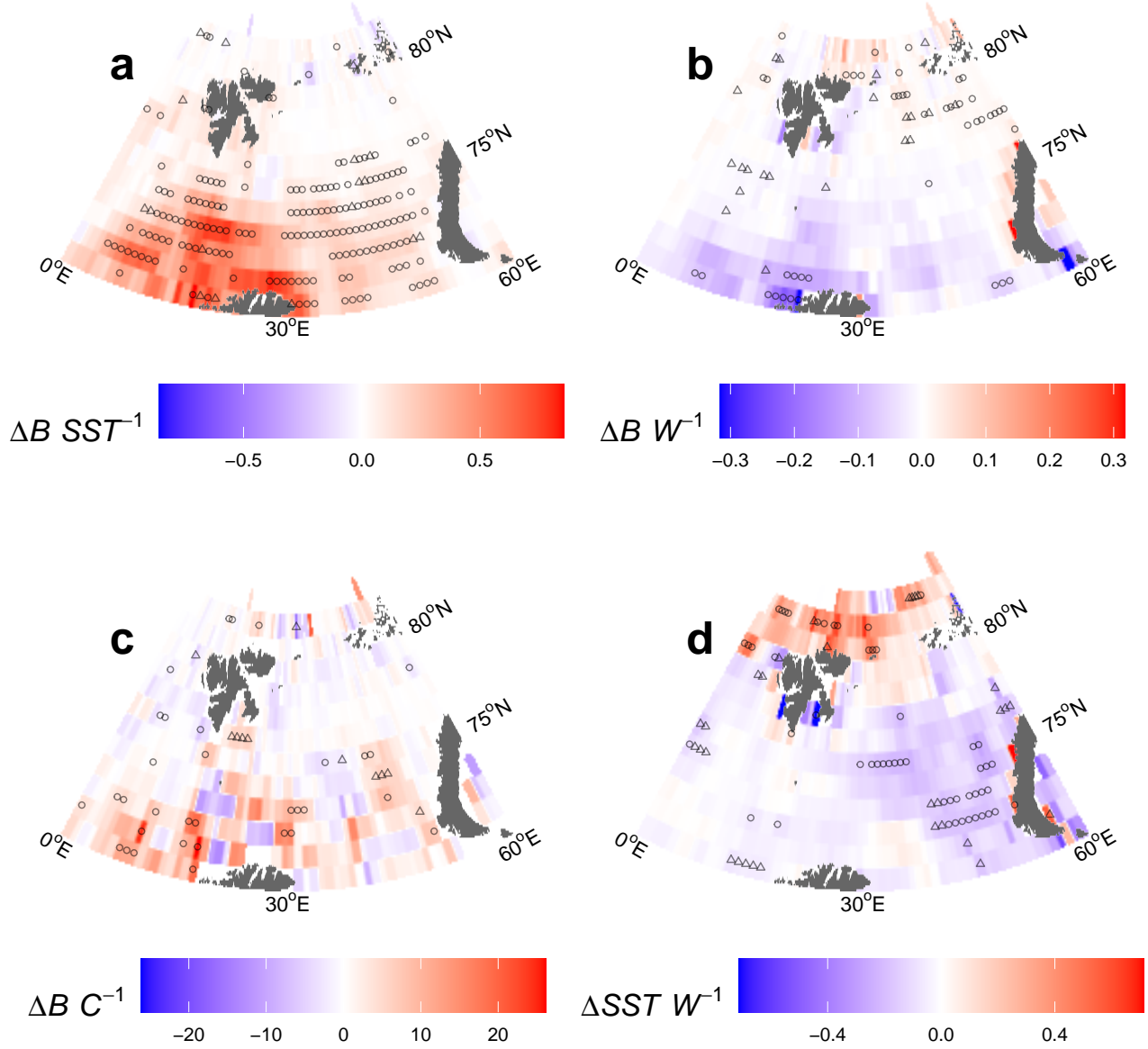


Figure S3: **Linear relationships, without masking coccolithophores:** Slopes of linear relationships. $[chl-a]$ (B) (mg m^{-3}), SST (Kelvin), windy days (W) and current speed (C) (m s^{-1}) are considered. (a) Biomass dependency on SST. (b) Biomass dependency on wind. (c) Biomass dependency on local currents. (d) SST dependency on wind. Grid cells with significant ($p < 0.05$) trends are marked with triangles when an autocorrelated fit is preferred, and circles when a standard fit is preferred. There is a strong positive relationship between biomass and SST, but not between biomass and wind. There is an ambiguous relationship of biomass and regional current speeds, and relationships between SST and winds vary between Atlantic and Arctic water masses. All data represent monthly integrations in September between 2002 and 2019.

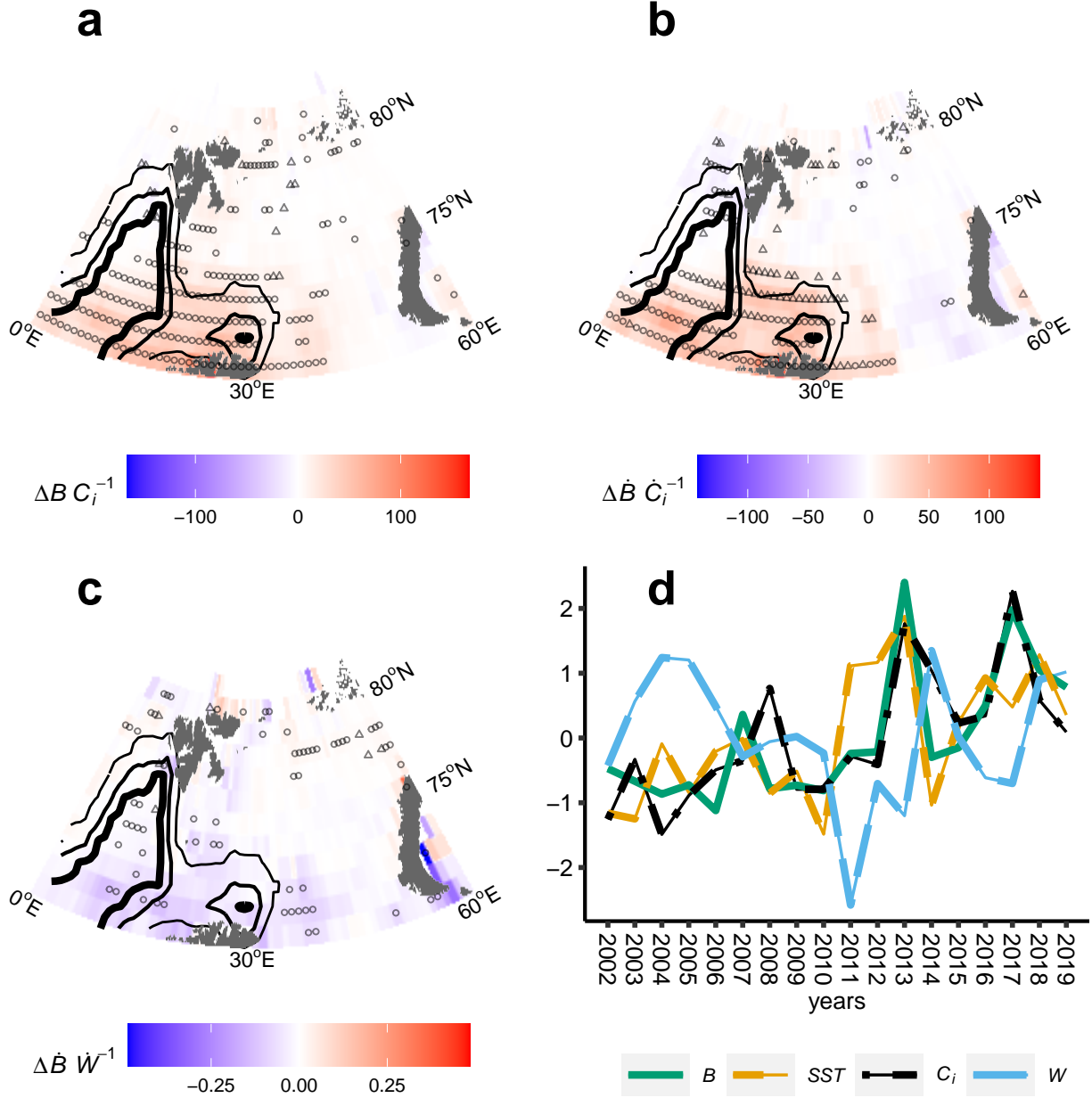


Figure S4: **Role of Atlantic inflow, without masking coccolithophores:** [*chl-a*] (B) (mg m^{-3}), inflow current speed (C_i) (ms^{-1}), inter-annual differences of [*chl-a*] (\dot{B}) ($\text{mg m}^{-3} \text{yr}^{-1}$), inflow current speed (\dot{C}_i) ($\text{ms}^{-1} \text{yr}^{-1}$), and windy days (\dot{W}), are considered. (a) Biomass dependency on Atlantic inflow. (b) inter-annual differences. (c) Inter-annual differences of biomass and wind. (d) Regional variance-normalised [*chl-a*], SST, inflow current speed and windy days are presented. Grid cells with significant ($p < 0.05$) trends are marked with triangles when an autocorrelated fit is preferred, and circles when a standard fit is preferred. Thin, medium and bold contours map the 5%, 50% and 95% occurrence intervals of the geographic distribution of Atlantic Water in the time-series, based on salinity ($>34.8\text{‰}$) and temperature ($>3^\circ\text{C}$). Strong positive relationships between biomass and Atlantic inflow currents are evident, especially within the region occupied by Atlantic Waters. Inter-annual variability in windiness anti-correlates with biomass. All data represent monthly integrations in September between 2002 and 2019.

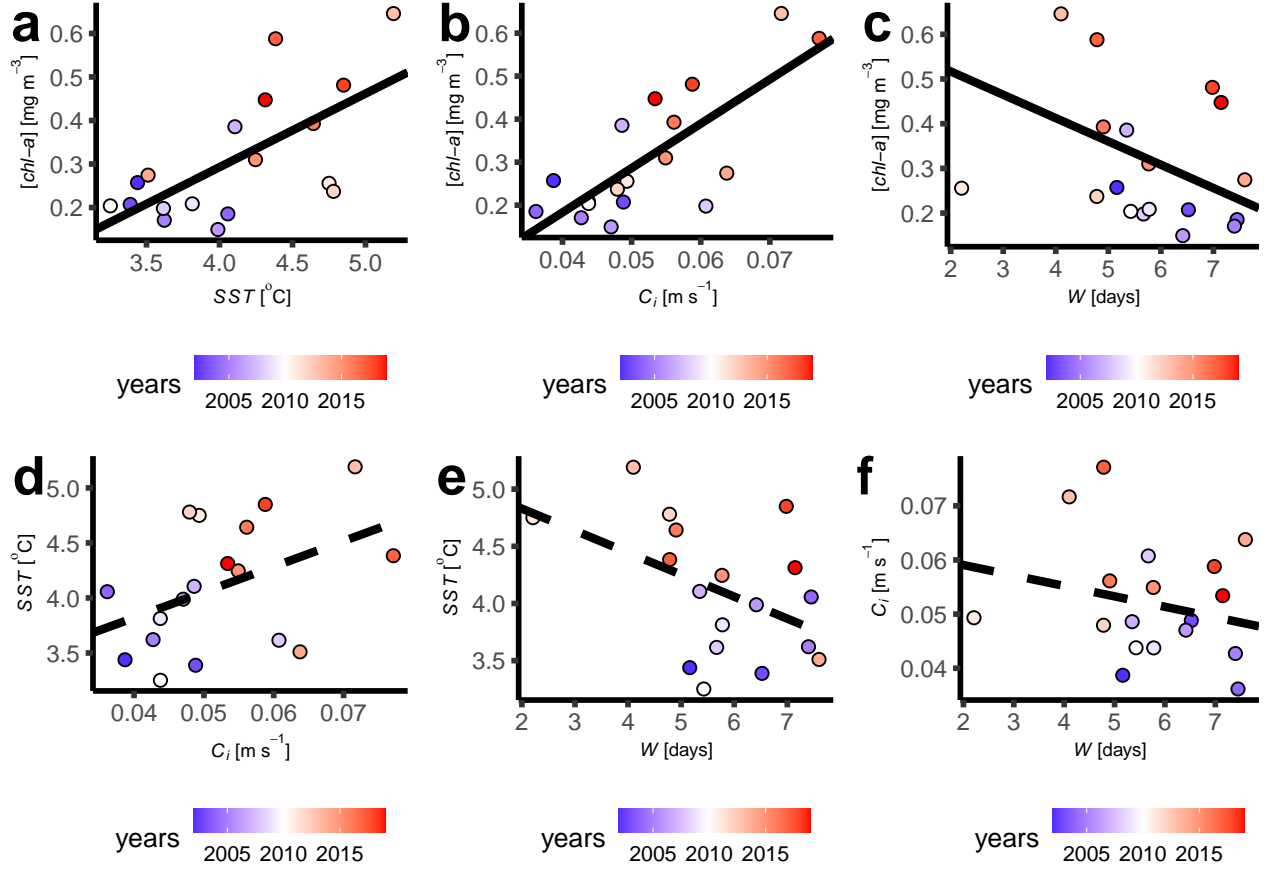


Figure S5: **Pairwise comparisons:** Visualisations of a selection of data and model fits from Table 2 (main manuscript). (C_i): Inflow current speed. (W): Windy days. (SST): Sea Surface Temperature. Solid lines indicate significance at $p < 0.05$, whereas dashed lines indicate insignificance. (a) Biomass dependency on SST . (b) Biomass dependency on C_i . (c) Biomass dependency on W . (d) SST dependency on C_i . (e) SST dependency on W . (f) C_i dependency on W .

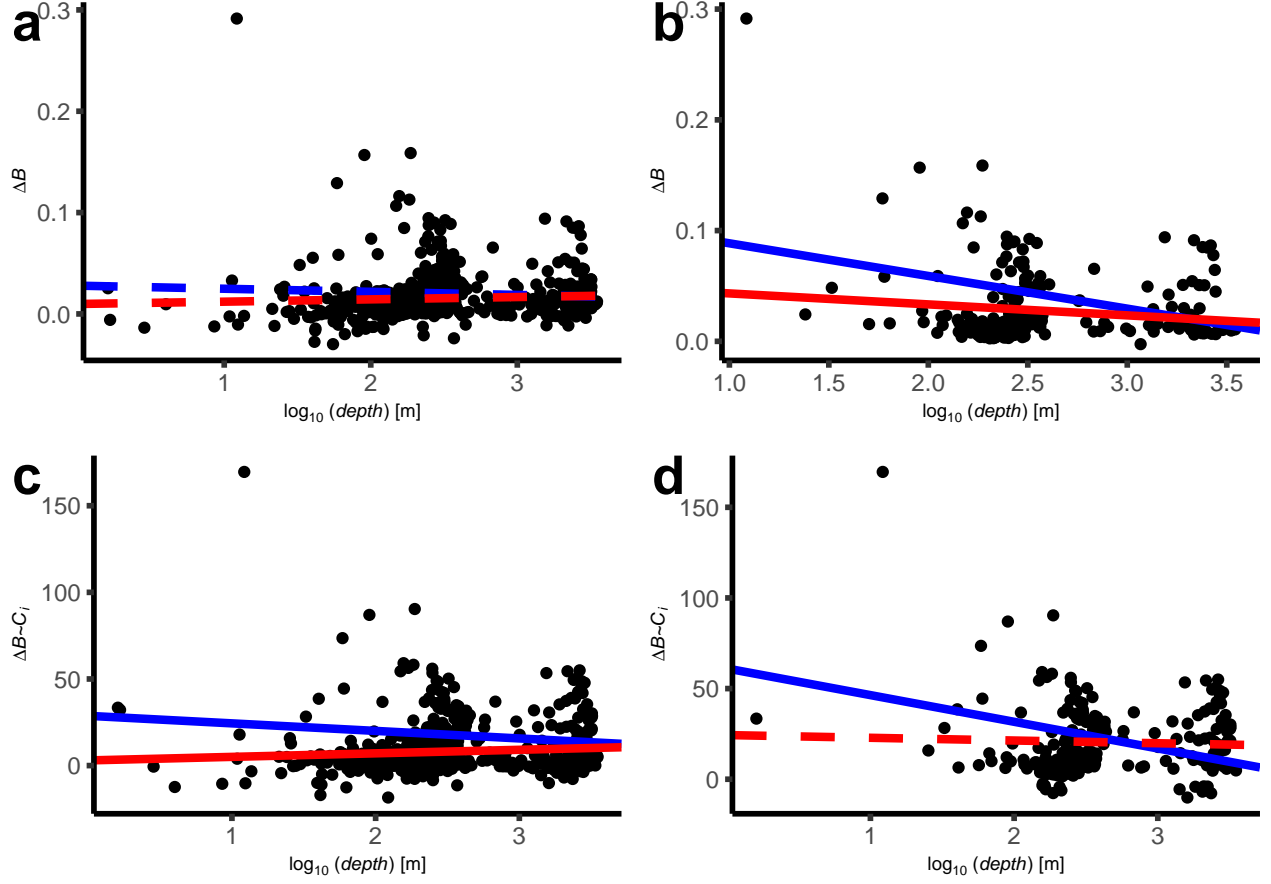


Figure S6: Ordinary Least Squares (red) and Generalised Least Squares (blue) fits, exploring the role of bathymetry in modulating inter-annual variation in autumn blooms. Solid lines indicate significance at $p < 0.05$, whereas dashed lines indicate insignificance. (a) Dependency of secular change in $[chl-a]$ (ΔB) upon the logarithm of bottom depth. (b) Identical to (a), but excluding grid-cells in which $[chl-a]$ has not changed significantly across the time-series. (c) Dependency of relationship of $[chl-a]$ to average inflow current speed ($\Delta B \sim C_i$) upon the logarithm of bottom depth. (d) Identical to (c), but excluding grid-cells in which $[chl-a]$ does not depend significantly upon C_i .

4 LITERATURE CITED

- Hansen K, Schmaltz J, Stevens J (2016) The Barents Sea Abloom. <https://earthobservatory.nasa.gov/images/88316/the-barents-sea-abloom> Accessed: 2020-03-03
- Kogeler J, Rey F (1999) Ocean colour and the spatial and seasonal distribution of phytoplankton in the Barents Sea. *Int J Remote Sens* 20(7):1303–1318
- Lewis K, Van Dijken G, Arrigo KR (2020) Changes in phytoplankton concentration now drive increased Arctic Ocean primary production. *Science* 369(6500):198–202
- Neukermans G, Oziel L, Babin M (2018) Increased intrusion of warming Atlantic water leads to rapid expansion of temperate phytoplankton in the Arctic. *Glob Change Biol* 24(6):2545–2553
- Orkney A, Platt T, Narayanaswamy BE, Kostakis I, Bouman HA (2020) Bio-optical evidence for increasing *Phaeocystis* dominance in the Barents Sea. *Philos Trans R Soc Lond, A* 378(2181):20190357
- Oziel L, Baudena A, Ardyna M, Massicotte P, Randelhoff A, Sallée JB, Ingvaldsen RB, Devred E, Babin M (2020) Faster Atlantic currents drive poleward expansion of temperate phytoplankton in the Arctic Ocean. *Nat Commun* 11(1):1–8
- Oziel L, Neukermans G, Ardyna M, Lancelot C, Tison JL, Wassmann P, Sirven J, Ruiz-Pino D, Gascard JC (2017) Role for Atlantic inflows and sea ice loss on shifting phytoplankton blooms in the Barents Sea. *J Geophys Res, C, Oceans* 122(6):5121–5139
- Pebesma EJ (2004) Multivariable geostatistics in S: the gstat package. *Comput Geosci* 30:683–691
- Pinheiro J, Bates D, DebRoy S, Sarkar D, R Core Team (2020) nlme: Linear and nonlinear mixed effects models. <https://CRANR-project.org/package=nlme> R package version 3.1-144
- Siswanto E (2020) Temporal variability of satellite-retrieved chlorophyll-a data in Arctic and subarctic ocean regions within the past two decades. *Int J Remote Sens* 41(19):7427–7445
- Smedsrud LH, Esau I, Ingvaldsen RB, Eldevik T, Haugan PM, Li C, Lien VS, Olsen A, Omar AM, Otterå OH, et al. (2013) The role of the Barents Sea in the Arctic climate system. *Rev Geophys* 51(3):415–449